# Coupling of an acoustic wave to shear motion due to viscous heating

Bin Liu and J. Goree
*Department of Physics and Astronomy, The University of Iowa, Iowa City, Iowa 52242, USA*

(Received 26 April 2016; accepted 22 June 2016; published online 21 July 2016)

Viscous heating due to shear motion in a plasma can result in the excitation of a longitudinal acoustic wave, if the shear motion is modulated in time. The coupling mechanism is a thermal effect: time-dependent shear motion causes viscous heating, which leads to a rarefaction that can couple into a longitudinal wave, such as an acoustic wave. This coupling mechanism is demonstrated in an electrostatic three-dimensional (3D) simulation of a dusty plasma, in which a localized shear flow is initiated as a pulse, resulting in a delayed outward propagation of a longitudinal acoustic wave. This coupling effect can be profound in plasmas that exhibit localized viscous heating, such as the dusty plasma we simulated using parameters typical of the PK-4 experiment. We expect that a similar phenomenon can occur with other kinds of plasma waves. *Published by AIP Publishing.* [http://dx.doi.org/10.1063/1.4956444]

## I. INTRODUCTION

Plasmas, in general, can sustain both longitudinal and transverse waves, sometimes at the same frequencies. One kind of wave can be converted into another by several mechanisms that are known, including linear mode conversion (for a wave propagating into a gradient in plasma density, for example)[1] as well as nonlinear coupling mechanisms such as Raman and Brillouin backscatter.[2] In this paper, we report another mechanism for the coupling of two waves: rarefaction arising from viscous heating.

In the presence of a velocity shear, viscous heat is produced at a rate

$$\dot{Q} \propto \eta\gamma^2. \tag{1}$$

Here, $\eta$ is a viscosity, and $\gamma \equiv du_x/dy$ is the transverse gradient of a hydrodynamic velocity $u_x$. If the velocity shear $\gamma$ is modulated in time, the viscous heat production will be similarly modulated. It is therefore possible for an oscillating wave with shear motion to result in an oscillating pattern of temperature variation. Likewise, it is possible for a pulsed shear motion to produce a pulsed temperature variation.

Viscous heating is certainly a well-known phenomenon in fluid mechanics. It is, for example, the energy loss mechanism for water flowing through a pipe. If a fluid has a shear that is spatially localized, one would expect heat to be generated mainly in the high-shear region. A localized hot spot could develop, unless thermal conduction is so rapid as to immediately flatten the spatial profile of the temperature. This rapid flattening indeed occurs in ordinary fluids such as water, so that localized hot spots due to viscous heating are not observed in those substances. On the other hand, certain plasmas may have a combination of strong viscous heating and small thermal conduction so that hot spots can occur, as was observed for the first time in a dusty plasma experiment.[3] This recent discovery leads us to search for wave-coupling effects due to localized viscous heating in dusty plasmas. We conduct this search using a three-dimensional (3D) electrostatic simulation of a dusty plasma.

A dusty plasma[4–17] is a mixture of electrons, ions, and small solid particles that are highly charged. It can also contain neutral gas. A flow of dust particles is often observed in dusty plasma experiments due to momentum imparted by an ion flux[18] or laser beams.[3,19–21] The charge on a dust particle is typically $-10^4 e$, for micron-size particles. With such a large charge, the collection of dust particles represents a strongly coupled plasma,[22] so that dust particles interact mostly with their nearest neighbors, as molecules do in a liquid. These strong Coulomb collisions can also have profound effects on transport processes, including viscosity[23] in the case of flowing dust particles.

Collective wave motion, both longitudinal and transverse, can be sustained in dusty plasmas. In a longitudinal wave, planar wavefronts propagate parallel to the oscillatory particle motion, and the collection of particles exhibits an oscillatory compression and rarefaction. This longitudinal wave is much like an acoustic wave, except that it exhibits dispersion at short wavelengths, due to the finite distances between dust particles.[24,25] In a transverse wave, there is a oscillatory shear motion, with particle velocity in the direction perpendicular to the wave propagation. These transverse waves are analogous to the S wave in seismology. In a liquid-like dusty plasma, the transverse wave propagates only a few interparticle spacings; it cannot have a long wavelength as the compressional wave can.[25,26] Both kinds of waves can be damped as they propagate, due to friction on the ambient neutral gas.[25]

Waves in dusty plasmas, as in other kinds of plasmas,[27] can, in general, be excited either thermally, by instabilities or some external manipulations. Spectra of thermally excited waves, or natural phonons, have been observed in two-dimensional[28] and one-dimensional[29] strongly coupled dusty plasmas; in a weakly coupled plasma, these thermal spectra are sometimes called normal modes.[27] Instabilities, such as those due to ion flows in the weakly coupled limit, have been shown experimentally to cause self-excitation of dust acoustic waves (DAWs).[30–35] Rosenberg *et al.*[36] derived a theory for waves spontaneously excited by a beam of dust particles

passing through a cloud of other dust particles. Particles moving at a supersonic speed can also excite Mach-cone like disturbances in dusty plasmas.[37–39] External excitation mechanisms that have been used to launch waves in a dusty plasma include an electrically modulated metal wire or electrode[24,40–42] and a modulated laser radiation pressure force.[43,44]

In this paper, we use a simulation to demonstrate yet another wave excitation mechanism, arising from localized viscous heating. In a simulation of a strongly coupled dusty plasma, we apply an impulsive force that drives a shear motion with a sudden onset. After a delay, we observe a longitudinal acoustic wave that propagates outwards from the edge of the flow. This excitation of the longitudinal wave occurs after a time delay that is consistent with the observed time scale for the localized heating of the dust component.

## II. METHOD

### A. Simulation

In our 3D simulation of a dusty plasma, pulsed particle motion is induced by an externally applied pulsed force. In an experiment, this external force could be provided by the radiation pressure force applied by a manipulation laser.[25]

We describe here a widely used model of dusty plasmas.[45] Dust particles are treated as point charges that interact electrostatically. Electrons and ions in the plasma provide Debye screening, with a screening length $\lambda_D$. The interaction between dust particles is binary and described by a Debye-Hückel (Yukawa) potential

$$\phi(r_{ij}) = \frac{Q^2}{4\pi\epsilon_0}\frac{\mathrm{e}^{-r_{ij}/\lambda_D}}{r_{ij}}, \tag{2}$$

where $r_{ij}$ is the separation between two particles $i$ and $j$. The particle charge $Q$ and the screening length $\lambda_D$ are prescribed parameters, chosen to mimic a particular experiment. The motion of electrons and ions is not simulated, so that the validity of this simulation is limited to disturbances of the dust component that have low frequencies and low amplitudes. Other effects we neglect in this simplified model include anisotropy in the potential (due to the ion flow wake, for example[46,47]) and electron depletion (which would alter the charge according to the local dust number density[48]). It is reasonable to neglect this depletion effect for our simulation, because we will perform the simulation under conditions where the dust number density will vary by less than 20%.

The equation of motion for a particle $i$ of mass $m$ in this simplified model is

$$m\ddot{\mathbf{r}}_\mathbf{i} = -\sum_j \nabla\phi_{ij} - \nabla\Phi - \nu_{\mathrm{gas}} m\dot{\mathbf{r}}_\mathbf{i} + \zeta_i(t) + \mathbf{F}. \tag{3}$$

The terms on the right hand side of Eq. (3) correspond to the electric interparticle repulsion as described by Debye-Hückel potential, the electrical force $-\nabla\Phi$ due to a prescribed electrostatic confinement in the $y$ and $z$ directions, the friction $-\nu_{\mathrm{gas}} m\dot{\mathbf{r}}_\mathbf{i}$ and the random forces $\zeta_i(t)$ both due to gas molecules, and finally the externally applied force $\mathbf{F}$ to drive a shear flow. We will choose to apply a non-zero $\mathbf{F}$ as a long pulse to a limited portion of the simulation cell. The pulse duration is of order $10^1\omega_p^{-1}$, so that the resulting shear motion couples effectively into the longitudinal wave. Here, $\omega_p = \sqrt{Q^2 n/\epsilon_0 m}$, where $n$ is the 3D number density of dust particles.

To simulate a long plasma shape, we use a periodic boundary condition in the $x$ direction. In the $y$ and $z$ directions, dust particles are electrostatically confined, as mentioned above. This configuration mimics a portion of the plasma volume in a long positive column. The simulation cell, Fig. 1, has dimensions of $L_x L_y L_z = 55 \times 33.8 \times 28.9\, a^3$, consisting $N = 12\,800$ particles. Here, $a$ is the Wigner-Seitz radius $a = (3/4\pi n)^{1/3}$.

### B. Simulation parameters

Our parameters were motivated by experiments with 3D dusty plasma clouds. Such 3D experiments are often performed under microgravity conditions. The PK-4 instrument,[49–51] now on orbit on the International Space Station (ISS), is a facility for performing such experiments. It is equipped with a manipulation laser beam along the $x$ direction, i.e., the axis of the plasma column. We chose our dust particle size and gas pressure to mimic experimental parameters in the PK-4 instrument. Our dust particles have a radius 3.43 $\mu$m and a mass $m = 2.55 \times 10^{-13}$ kg. The gas is neon, with a relatively low pressure of 2.5 Pa. At this pressure, a dust particle experiences a gas drag force $F_{\mathrm{gas}}$ characterized by the frictional constant $\nu_{\mathrm{gas}} \equiv F_{\mathrm{gas}}/m\dot{r} = 2.6\,\mathrm{s}^{-1}$. Other parameters include the inverse time scale $\omega_p = 157\,\mathrm{s}^{-1}$ and $\kappa \equiv a/\lambda_D = 2.4$, which can be satisfied by a particle charge $Q = -8520\,e$, equilibrium dust number density $n_0 = 3 \times 10^4\,\mathrm{cm}^{-3}$ or $a = 0.02$ cm, and screening length $\lambda_D = 0.0083$ cm.

The simulation was initialized, before applying the external force, with parameters chosen so that our dust particle cloud behaves collectively like a liquid. The coupling parameter[52] is $\Gamma \equiv Q^2/4\pi\epsilon_0 a k_B T_0 = 310$, for the initial dust kinetic temperature $T_0$ and number density $n_0$. We chose this value of $\Gamma$ so that $T_0 = 2\,T_m$, where $T_m$ is the melting point of a Yukawa liquid,[53] at $\kappa = 2.4$. The liquid-like structure within the dust cloud is verified by the pair correlation

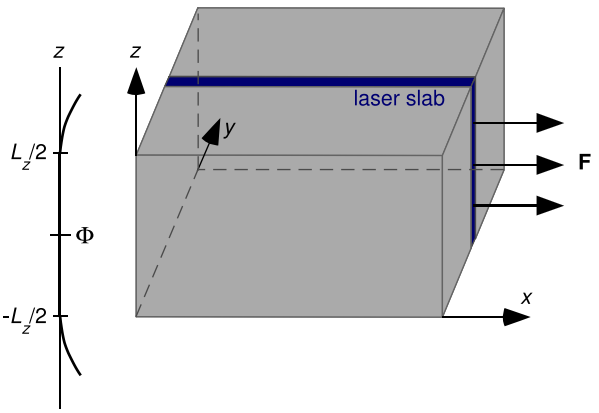


FIG. 1. Simulation cell. Particles are confined by a flattened potential well in the $y$ and $z$ directions. The boundary in the $x$ direction is periodic. An external force $\mathbf{F}$ is applied with a uniform distribution inside a central "laser slab."

function $g(r)$ shown in Fig. 2. For our conditions, the kinematic viscosity is $\nu = 0.068\, a^2\omega_p$, which we determined using the Green-Kubo method[54] with our simulation data.

The sound speed was $c_l = 0.26 \pm 0.03\, a\omega_p$ for the longitudinal waves. We obtained this value by computing the natural phonon spectrum[28] from our data for the undisturbed 3D dusty plasma.

After the initialization, a non-zero external force $\mathbf{F} = F\hat{x}$ was applied to create an impulsive shear flow. The external force was applied locally to particles that were positioned within $|y| \leq 0.84a$, which we term the "laser slab." The external force was modulated as a pulse, starting at $t\omega_p = 0$ and ending at $t\omega_p = 14$. To yield a flow velocity of order $10^1$ mm/s, as has been observed in PK-4,[51] the amplitude of the force was chosen to be $0.096\, m\omega_p^2 a$. In our simulation, this flow velocity was supersonic, as compared to $c_l = 0.26\, a\omega_p$.

We consider here only the early stages of the impulsive shear flow, before any vortices can develop. We simulate times $\lesssim L_y/2c_l$, i.e., up to the time required for a longitudinal sound wave to propagate a distance halfway across the simulation cell. This early stage of response was too early for the flow to be described as laminar or turbulent, but nevertheless for the purpose of completing our list of parameters, we can characterize the Reynolds number for the flow. We calculate this using $Re = \Delta u_x L/\nu$, with $\Delta u_x = 1.0 a\omega_p$, which is the largest observed difference in flow velocity at $y = 0$ as compared to $y = L_y/2$. The value of $Re$ depends on the choice of the length scale $L$; we find $Re = 800$ or 22, for $L = L_x$ or $L = u_x/\gamma = 1.5a$, respectively, where the latter is a typical scale length for the shear.

### C. Computing hydrodynamic quantities

Our simulation was performed in the particle paradigm, by tracking the motion of individual particles. Our analysis, however, requires a description in the hydrodynamic paradigm. We will report three hydrodynamic quantities: number density $n$, flow velocity $\mathbf{u}$, and kinetic temperature $T$. These were obtained by averaging, respectively, the number of particles, the particle momentum, and the square velocity $(\dot{\mathbf{r}}_\mathbf{i} - \mathbf{u})^2$. In the presence of the strong shear flow, the mean square velocity was found to be anisotropic, with higher values for the $x$ direction; we will report only values for the $y$ direction, since it is less affected by the flow. The averaging was always done within a spatial bin. We used 41 rectangular bins, each with a narrow extent of $0.84\, a$ in the $y$ direction to provide spatial resolution. These bins extended across the entire simulation cell in the $x$ and $z$ directions.

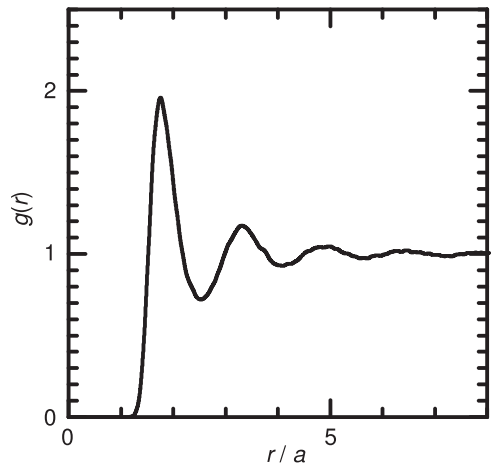


FIG. 2. Pair correlation function indicating a liquid-like structure of the dust cloud, before applying the external force $\mathbf{F}$.

### D. Units

Normalized units used in this paper are as follows. Distance, time, and force are normalized by $a$, $\omega_p^{-1}$, and $m\omega_p^2 a$, respectively. The flow velocity is reported as a Mach number $u_x/c_l$ and $u_y/c_l$. The temperature and density are normalized by their initial values $T_0$ and $n_0$, before the pulsed force is applied.

## III. RESULT

Our main results are observations of the excitation of a compressional acoustic pulse coinciding with localized heating and rarefaction. These are all observed at a time that is delayed after the onset of an impulsive shear flow. We find that the compressional pulse propagates away from the thin laser slab, where it is excited. Its wavefront is observed to be planar. The heating and rarefaction are found to occur at nearly the same location and time as the excitation of the compressional wave, suggesting the viscous heating mechanism as the cause of the excitation. We present details of these results below.

### A. Initial response

The space-time diagrams in Fig. 3 characterize the flow, heating, and density variation, in response to the impulsive force. After the force is turned on, a flow begins to develop, and the hydrodynamic parameters begin to change. These changes are most profound near the laser slab.

#### 1. Flow

The flow in the $x$ direction, i.e., the direction of the laser force, starts without a delay when the force is turned on, and it gradually accelerates, as seen in Fig. 3(a). This initial acceleration is almost constant, meaning the flow velocity increases linearly with time. A simple calculation shows that this initial acceleration is 80% of what would be expected due to the laser force alone; the remainder must be attributed to a loss of momentum in the laser slab due to viscosity or gas friction. After the laser force is turned off, the flow $u_x$ reaches a maximum speed of $4.1\, c_l$ at $t\omega_p \approx 14$ inside the laser slab. Outside the laser slab, the flow velocity $u_x$ diminishes with increasing $|y|$, meaning that there is a shear. This shear is most profound near the two edges of the laser slab.

#### 2. Heating

The kinetic temperature of the particles begins to increase in the laser slab and the surrounding region after a noticeable delay of $t\omega_p \approx 7$, as seen in Fig. 3(b). The heating is substantial: the kinetic temperature $T$, measured from

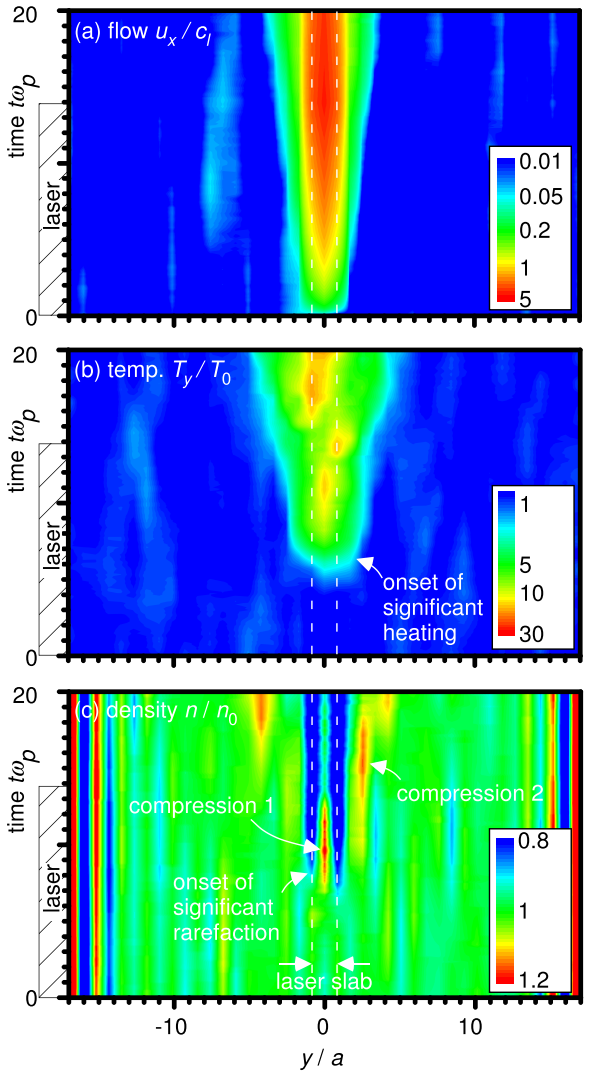


FIG. 3. Space-time diagrams showing shear-flow induced heating and rarefaction. (a) A shear flow pattern $u_x(y)$ develops at $t > 0$, starting almost immediately when an external force is applied. (b) The temperature starts to increase rapidly after a delay; the onset of noticeable heating is at $t\omega_p \approx 7$. The temperature increase is attributed to viscous heating. Both the shear flow and the heating are spatially localized, mostly within the laser slab. (c) The density undergoes a rarefaction, at the two edges of the laser slab, after a delay similar to that for temperature. The color scales are logarithmic in (a) and (b), but linear in (c).

absolute zero, increases by a factor as large as 30, as compared to the initial value $T_0$ which was already high enough to sustain a liquid condition. This temperature increase is due to viscous heating, in competition with heat removal by conduction and gas friction.[3]

### 3. Rarefaction and compression

Rarefaction, i.e., a decrease in particle number, is seen in Fig. 3(c) at about the same delayed time as the temperature increase. This change in the number density is more spatially localized than is the change in temperature. The rarefaction starts at the two edges of the laser slab, and it expands over time in the $\pm y$ directions. The change in number density is less profound than for the temperature, with a maximum variation of about $\pm 20\%$. The coincidence that the rarefaction begins to develop at the same delayed time as the heating suggests that the rarefaction arises from the heating, although we have not modeled this process using the hydrodynamic quantities.

The particles that are removed during the rarefaction must of course appear elsewhere. This development can be identified in the two short-lived density compressions in Fig. 3(c), which we mark as "compression 1" and "compression 2" inside and outside the laser slab, respectively. This combination of impulsive compression and rarefaction is of interest for explaining the acoustic pulse propagation that we will present in Sec. III C.

Further details of the transverse flow responsible for the "compression 1" event of Fig. 3(c) can be seen in Fig. 4, which shows a time series of the transverse velocity $u_y$. The data in Fig. 4 are for a particular location, $y = 0.84\,a$, which is slightly outside the laser slab. A negative value of $u_y$ indicates an inward flow, toward the center of the laser slab, and this can be seen for $t\omega_p \lesssim 6$. This inward flow causes the short-lived "compression 1" inside the laser slab, for $7 \lesssim t\omega_p \lesssim 10$.

Figure 4 also shows some details about the transverse flow responsible for the "compression 2" event. An outflow from the laser slab is indicated by a positive value of $u_y$, and this is seen for $7 \lesssim t\omega_p \lesssim 20$. This brief outflow coincides with the development of the "compression 2" feature in Fig. 3(c).

### B. Long time response

Although it is not one of our main results, we will next consider the motion for a longer time interval, $0 < t\omega_p < 70$. As seen in Fig. 5(a), after the laser force is turned off at $t\omega_p = 14$, the flow $u_x$ does not cease immediately. The inertia of the dust particles sustains the flow, diminishing only gradually due to gas friction and viscous dissipation. About 2% of the peak velocity remains at $t\omega_p \approx 70$. During this entire

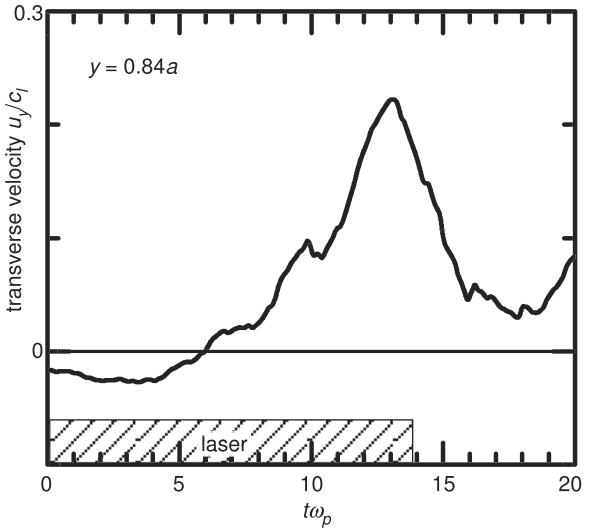


FIG. 4. Transverse flow near the laser slab's edge, at $y = 0.84\,a$. In this time series of transverse velocity $u_y$, a positive value of $u_y$ indicates that particles are expelled from the laser slab, which helps explain the rarefaction observed in Fig. 3(c).

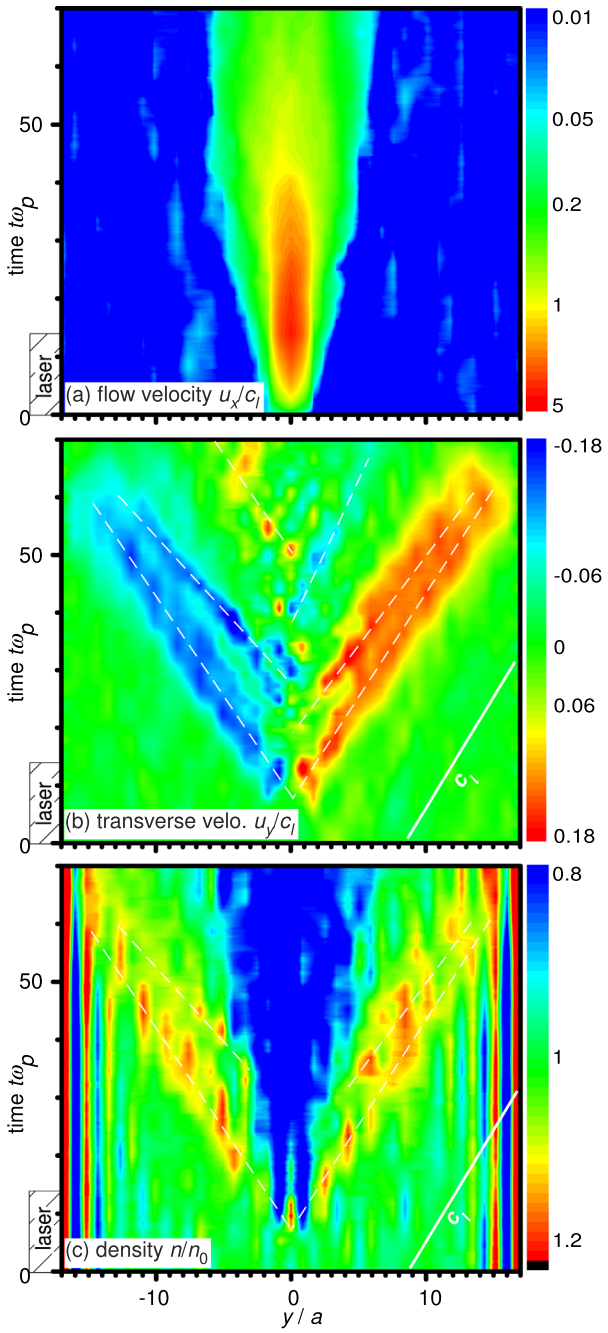


FIG. 5. Space-time diagrams, over a longer time than in Fig. 3. The impulsive shear flow is shown in (a). Compressional wavefronts are revealed in (b) for the transverse velocity and (c) for the dust number density. These wavefronts correspond to propagation in the $\pm y$ directions. We have marked crests and troughs with dashed lines. The vertex of the crests at $t\omega_p \approx 7$ indicates the wave excitation time, which is delayed as compared to the start of the flow. To help judge the speed, in the lower corners we have drawn a solid line with a slope corresponding to the longitudinal sound speed. The color scales are logarithmic in (a), but linear in (b) and (c).

time, as seen in Fig. 5(a), the flow pattern broadens in the $\pm y$ directions, due to the viscous diffusion of momentum; this diffusion causes momentum in the $x$ direction, which was previously concentrated in the laser slab, to gradually shift to larger values of $|y|$.

In addition to the flow $u_x$, the space-time diagrams in Fig. 5 also show the transverse velocity $u_y$ and the number density of particles. In the number density plot of Fig. 5(c), we see that the rarefaction region continues to broaden with time, during this entire observation time.

### C. Acoustic pulse observation

#### 1. Wavefront characterization

Our main results are the distinctive wavefronts seen in the space-time diagrams in Figs. 5(b) and 5(c). These wavefronts have a V-shaped appearance in the space-time diagram, indicating a planar wavefront propagating outward from the laser slab, at a steady speed. The propagation is along the $\pm y$ axis.[55]

The pulsed wave that we observe in Figs. 5(b) and 5(c) can be identified as longitudinal, i.e., compressional, based on the directions of propagation and particle motion. As mentioned above, the propagation direction is in the $\pm y$ directions. The particles have motion along both the $x$ and $y$ axes, but the wave motion is seen only in $u_y$ in Fig. 5(b), not in $u_x$ in Fig. 5(a). Thus, the particle motion associated with the wave is along the same axis as the direction of propagation.

The compressional wave has an amplitude that is large enough to detect easily, but it is not extreme. The wave has at most a 20% variation in the density, as compared to the equilibrium value.[56] Nevertheless, the wave is strong enough to be easily identified in the space-time diagrams. It is not damped significantly; it reaches the edge of the simulation cell without significant damping. Because the motion in this wave is compressional and not shear, we expect that it will not be damped much by viscous dissipation. The main dissipation mechanism for this compressional wave is probably gas friction.

The speed of the wave propagation is comparable (but not exactly the same) as the sound speed $c_l$. To demonstrate this, in Figs. 5(b) and 5(c), we have marked some wavefront crests and troughs with dashed lines. They have roughly the same slope as the solid line, which we provide for reference to indicate the sound speed $c_l$. There is, however, some variation in the speed of the wavefronts, as seen by the varying slopes of the dashed lines, ranging from $0.2a\omega_p$ to $0.39a\omega_p$.

#### 2. Delay of wavefront development

The timing of the wave's generation will be helpful in explaining the excitation mechanism. We find that the compressional wavefronts do not develop instantaneously when the shear flow begins. They develop after a delay, as seen in the space-time diagram of Fig. 5(b). In that diagram, the first vertex in the wavefronts occurs at $t\omega_p \approx 7$. We note that this time coincides with the time that significant heating, compression, and rarefaction have developed.

## IV. VISCOUS-HEATING EXCITATION MECHANISM

### A. Pulsed excitation

We explain the pulse excitation as the result of localized viscous heating. The steps in this mechanism are as follows.

- A shear flow begins, resulting in viscous heating, Eq. (1), that causes the temperature to increase gradually with time.
- A hot spot then develops at the edge of the laser slab, where the gradient in the flow velocity is largest.
- At the same location, the number density undergoes a rarefaction; this rarefaction develops not instantaneously, but gradually, just as the temperature does.
- The particles expelled from this rarefaction layer move to compression layers that are parallel to the rarefaction layer.
- The emergence of these parallel layers of compression and rarefaction is how a planar wavefront develops.
- Thereafter, this wavefront propagates outward, as a pulse-like compression.

Further study of the excitation mechanism could be performed by investigating the effect of varying force amplitudes, which we have not done in this paper. If the mechanism we propose is valid (in other words if the compressional wave we observed is indeed the result of a momentary rarefaction arising from viscous heating), then we expect there will be no threshold or minimum force to excite the compressional wave. At higher laser forces than in our simulation, there are several possible effects that we have not explored. One effect is that shear thinning (a diminishment of viscosity with increasing shear) could cause the wave excitation amplitude to vary more weakly than the linear response that one might otherwise expect. Another effect might be that the heated region could expand spatially to a larger extent, thereby affecting the coupling into short vs long wavelength compressional waves.

### B. Sinusoidal excitation

Beyond the pulsed waves that we observed in our simulation, we suggest that the same mechanism could result in sinusoidal excitation of a longitudinal wave. The requirements would be as follows. There must be an oscillating shear motion, whether associated with a wave or not. The frequency must be low, to allow thermal effects to accumulate. To achieve significant localized viscous heating, the Brinkman number must be of order unity, or at least not an extremely small number, and this requires significant viscosity.[3] Finally, it would probably be necessary to excite the sinusoidal shear motion *in-situ* rather than require a shear wave to propagate from a distant source, because in the latter case the shear wave would be damped by the viscosity. We expect that these requirements could all be met in a strongly coupled dusty plasma if the laser excitation scheme is configured with sinusoidal laser excitation.

Besides dusty plasmas, we expect that other kinds of plasmas could exhibit our viscous heating mechanism for wave excitation. For example, fast and slow Alfvén waves can propagate at the same frequency in a magnetized plasma, and they can have a low frequency. If the slow wave could be locally excited within a viscous magnetized plasma, it could be converted partially into a fast wave, which then propagates away from this excitation region. However, for waves in magnetized plasmas, our literature search did not identify previous papers presenting this viscous heating mechanism.

## V. SUMMARY

A longitudinal acoustic pulse was excited by an impulsive shear flow in a simulation of a 3D strongly coupled dusty plasma. The presence of the longitudinal pulse was seen in space-time diagrams of velocity and density. The heating and rarefaction appeared in the diagrams for temperature and density. The longitudinal pulse originated not at the time that the shear flow began, but later when the effects of heating and rarefaction had accumulated. Based on this timing, and the recently discovered tendency of a dusty plasma to exhibit significant localized viscous heating, we hypothesize that the wave excitation mechanism is essentially thermal. An impulsive shear motion causes an onset of viscous heating, which in turn results in a pulsed rarefaction that can launch a pulsed compressional wave. This compressional wave propagates in a direction perpendicular to the shear flow.

We expect that future experiments can test the prediction based on our simulation that the sudden onset of a shear flow can excite compressional pulses that propagate perpendicular to the flow. The PK-4 instrument, now on the International Space Station, is well suited for such an experimental test because it allows for a modulated laser manipulation similar to the one in our simulation. The main difference, as compared to our simulation, is that the laser beam cross section in PK-4 is circular rather rectangular. Observing the propagation of such a compressional pulse could have applications, such as allowing the experimenter to extract dusty plasma parameters, for example, the particle charge $Q$ if the screening length and number density are known.

## ACKNOWLEDGMENTS

This work was supported by NASA and the U. S. Department of Energy.

[1]T. H. Stix, *Waves in Plasmas* (Springer-Verlag, New York, 1992).
[2]P. M. Bellan, *Fundamentals of Plasma Physics* (University Press, New York, 2006).
[3]Y. Feng, J. Goree, and B. Liu, Phys. Rev. Lett. **109**, 185002 (2012).
[4]H. Thomas, G. E. Morfill, V. Demmel, J. Goree, B. Feuerbacher, and D. Mohlmann, Phys. Rev. Lett. **73**, 652 (1994).
[5]J. H. Chu and I. Lin, Phys. Rev. Lett. **72**, 4009 (1994).
[6]A. Melzer, A. Homann, and A. Piel, Phys. Rev. E **53**, 2757 (1996).
[7]W. T. Juan and I. Lin, Phys. Rev. Lett. **80**, 3073 (1998).
[8]P. K. Shukla and A. A. Mamun, *Introduction to Dusty Plasma Physics* (Institute of Physics, Bristol, 2002).
[9]B. Liu, J. Goree, V. Nosenko, and L. Boufendi, Phys. Plasmas **10**, 9 (2003).
[10]Y. Feng, J. Goree, and B. Liu, Rev. Sci. Instrum. **78**, 053704 (2007).
[11]O. Ishihara, J. Phys. D: Appl. Phys. **40**, R121 (2007).
[12]A. Melzer and J. Goree, in *Low Temperature Plasmas: Fundamentals, Technologies and Techniques*, 2nd ed., edited by R. Hippler, H. Kersten, M. Schmidt, and K. H. Schoenbach (Wiley-VCH, Weinheim, 2008), p. 129.
[13]G. E. Morfill and A. V. Ivlev, Rev. Mod. Phys. **81**, 1353 (2009).
[14]V. E. Fortov and G. E. Morfill, *Complex and Dusty plasma: From Laboratory to Space* in Series in Plasma Physics (CRC Press, New York, 2009).
[15]T. M. Flanagan and J. Goree, Phys. Rev. E **80**, 046402 (2009).

[16]A. Piel, *Plasma Physics* (Springer, Heidelberg, 2010).
[17]M. Bonitz, C. Henning, and D. Block, Rep. Prog. Phys. **73**, 066501 (2010).
[18]T. Bockwoldt, O. Arp, K. O. Menzel, and A. Piel, Phys. Plasmas **21**, 103703 (2014).
[19]V. Nosenko and J. Goree, Phys. Rev. Lett. **93**, 155004 (2004).
[20]P. Hartmann, A. Zs. Kovács, A. M. Douglass, J. C. Reyes, L. S. Matthews, and T. W. Hyde, Phys. Rev. Lett. **113**, 025002 (2014).
[21]A. Gavrikov, I. Shakhova, A. Ivanov, O. Petrov, N. Vorona, and V. Fortov, Phys. Lett. A **336**, 378 (2005).
[22]*Strongly Coupled Coulomb Systems*, edited by G. J. Kalman, K. B. Blagoev, and M. Rommel (Plenum Press, New York, 1998).
[23]K. Y. Sanbonmatsu and M. S. Murillo, Phys. Rev. Lett. **86**, 1215 (2001).
[24]J. B. Pieper and J. Goree, Phys. Rev. Lett. **77**, 3137 (1996).
[25]S. Nunomura, J. Goree, S. Hu, X. Wang, and A. Bhattacharjee, Phys. Rev. E **65**, 066402 (2002).
[26]V. Nosenko, J. Goree, and A. Piel, Phys. Rev. Lett. **97**, 115001 (2006).
[27]F. Anderegg, N. Shiga, J. R. Danielson, D. H. E. Dubin, C. F. Driscoll, and R. W. Gould, AIP Conf. Proc. **606**, 253 (2002).
[28]S. Nunomura, J. Goree, S. Hu, X. Wang, A. Bhattacharjee, and K. Avinash, Phys. Rev. Lett. **89**, 035001 (2002).
[29]B. Liu and J. Goree, Phys. Rev. E **71**, 046410 (2005).
[30]R. L. Merlino, A. Barkan, C. Thompson, and N. D'Angelo, Phys. Plasmas **5**, 1607 (1998).
[31]A. Piel, O. Arp, M. Klindworth, and A. Melzer, Phys. Rev. E **77**, 026407 (2008).
[32]T. M. Flanagan and J. Goree, Phys. Plasmas **17**, 123702 (2010).
[33]R. L. Merlino, J. R. Heinrich, S. H. Kim, and J. K. Meyer, Plasma Phys. Control. Fusion **54**, 124014 (2012).
[34]W. D. Suranga Ruhunusiri and J. Goree, Phys. Rev. E **85**, 046401 (2012).
[35]J. D. Williams, IEEE Trans. Plasmas **41**, 788 (2013).
[36]M. Rosenberg, G. J. Kalman, S. Kyrkos, and Z. Donko, J. Phys. A: Math. Gen. **39**, 4613 (2006).
[37]D. Samsonov, J. Goree, Z. W. Ma, A. Bhattacharjee, H. M. Thomas, and G. E. Morfill, Phys. Rev. Lett. **83**, 3649 (1999).
[38]M. Schwabe, K. Jiang, S. Zhdanov, T. Hagl, P. Huber, A. V. Ivlev, A. M. Lipaev, V. I. Molotkov, V. N. Naumkin, K. R. Sütterlin, H. M. Thomas, V. E. Fortov, G. E. Morfill, A. Skvortsov, and S. Volkov, EPL **96**, 55001 (2011).
[39]D. I. Zhukhovitskii, V. E. Fortov, V. I. Molotkov, A. M. Lipaev, V. N. Naumkin, H. M. Thomas, A. V. Ivlev, M. Schwabe, and G. E. Morfill, Phys. Plasmas **22**, 023701 (2015).
[40]N. P. Oxtoby, J. F. Ralph, C. Durniak, and D. Samsonov, Phys. Plasmas **19**, 013708 (2012).
[41]S. Khrapak, D. Samsonov, G. Morfill, H. Thomas, V. Yaroshenko, H. Rothermel, T. Hagl, V. Fortov, A. Nefedov, V. Molotkov, O. Petrov, A. Lipaev, A. Ivanov, and Y. Baturin, Phys. Plasmas **10**, 1 (2003).
[42]D. Samsonov, S. K. Zhdanov, R. A. Quinn, S. I. Popel, and G. E. Morfill, Phys. Rev. Lett. **92**, 255004 (2004).
[43]A. Melzer, S. Nunomura, D. Samsonov, Z. W. Ma, and J. Goree, Phys. Rev. E **62**, 4162 (2000).
[44]V. Nosenko, S. Nunomura, and J. Goree, Phys. Rev. Lett. **88**, 215002 (2002).
[45]Y. Feng, J. Goree, B. Liu, and E. G. D. Cohen, Phys. Rev. E **84**, 046412 (2011).
[46]F. Melandsø and J. Goree, Phys. Rev. E **52**, 5312 (1995).
[47]A. Melzer, V. A. Schweigert, and A. Piel, Phys. Rev. Lett. **83**, 3194 (1999).
[48]O. Havnes, T. K. Aanesen, and F. Melandsø, J. Geophys. Res. **95**, 6581, doi:10.1029/JA095iA05p06581 (1990).
[49]V. Fortov, G. Morfill, O. Petrov, M. Thoma, A. Usachev, H. Hoefner, A. Zobnin, M. Kretschmer, S. Ratynskaia, M. Fink, K. Tarantik, Y. Gerasimov, and V. Esenkov, Plasma Phys. Control. Fusion **47**, B537 (2005).
[50]M. H. Thoma, H. Hofner, M. Kretschmer, S. Ratynskaia, G. E. Morfill, A. Usachev, A. Zobnin, O. Petrov, and V. Fortov, Microgravity Sci. Technol. **18**, 47 (2006).
[51]S. A. Khrapak, S. Ratynskaia, A. V. Zobnin, A. D. Usachev, V. V. Yaroshenko, M. H. Thoma, M. Kretschmer, H. Höfner, G. Morfill, O. F. Petrov, and V. E. Fortov, Phys. Rev. E **72**, 016406 (2005).
[52]S. Ichimaru, Rev. Mod. Phys. **54**, 1017 (1982).
[53]S. Hamaguchi, R. T. Farouki, and D. H. E. Dubin, Phys. Rev. E **56**, 4671 (1997).
[54]J. P. Hansen and I. R. McDonald, *Theory of Simple Liquids*, 2nd ed. (Academic Press, San Diego, 1986).
[55]In Fig. 5(b), all the wavefronts appear to emerge from $y = 0$, corresponding to the laser slab. For propagation to the right $(+y)$ vs left $(-y)$, the first wavefronts emerge simultaneously, but later wavefronts emerge at differing times on the two sides. We have no explanation for this timing variation.
[56]This 20% maximum amplitude is small enough that nonlinear effects are probably not dominant, but we have not performed any tests to assess the role of nonlinearity in the wave propagation. In the absence of any signature of nonlinear effects, we refer to the compressional wavefronts in our simulation as pulsed waves, not as shocks.